RSC Advances

This is an *Accepted Manuscript*, which has been through the Royal Society of Chemistry peer review process and has been accepted for publication.

Accepted Manuscripts are published online shortly after acceptance, before technical editing, formatting and proof reading. Using this free service, authors can make their results available to the community, in citable form, before we publish the edited article. This *Accepted Manuscript* will be replaced by the edited, formatted and paginated article as soon as this is available.

You can find more information about *Accepted Manuscripts* in the Information for Authors.

Please note that technical editing may introduce minor changes to the text and/or graphics, which may alter content. The journal's standard Terms & Conditions and the Ethical guidelines still apply. In no event shall the Royal Society of Chemistry be held responsible for any errors or omissions in this *Accepted Manuscript* or any consequences arising from the use of any information it contains.

ROYAL SOCIETY OF CHEMISTRY

www.rsc.org/advances

Photoluminescence Tuning via Energy Transfer in the Eu-doped $Ba_2(Gd,Tb)_2Si_4O_{13}$ Solid-Solution Phosphors

Jun Zhou[a,b], Zhiguo Xia[*a], Marco Bettinelli[c], Quanlin Liu[a]

[a] *The Beijing Municipal Key Laboratory of New Energy Materials and Technologies, School of Materials Sciences and Engineering, University of Science and Technology Beijing, Beijing 100083, China*

[b]*School of Materials Sciences and Technology, China University of Geosciences, Beijing 100083, China*

[c]*Luminescent Materials Laboratory, DB, Univ. Verona, and INSTM, UdR Verona, Strada Le Grazie 15, 37134 Verona, Italy*

*** Corresponding author:**

Zhiguo Xia

E-mail: **xiazg@ustb.edu.cn**

School of Materials Sciences and Engineering, University of Science and Technology Beijing, Beijing 100083, China

Tel. : +86-10-8237-7955; Fax. : +86-10-8237-7955

RSC Advances Accepted Manuscript

Abstract: We report on the phase formation of $Ba_2(Gd,Tb)_2Si_4O_{13}$ solid-solution, and the coexistence of Eu^{2+}/Eu^{3+} was identified after Eu ions doping although the samples were prepared in a reducing atmosphere. Under 377 nm near-ultraviolet (UV) light excitation, $Ba_2Tb_2Si_4O_{13}$ exhibits the characteristic emission originating from Tb^{3+} corresponding to $^5D_4$-$^7F_{6, 5, 4, 3}$ transitions; whereas $Ba_2Tb_2Si_4O_{13}$:Eu emits bright red emission from Eu^{3+} with peaks around 594, 613 and 623 nm. Accordingly, photoluminescence tuning of the Eu-doped $Ba_2(Gd,Tb)_2Si_4O_{13}$ phosphors has been realized from the green, yellow, orange, to red emission light. Decay time and time-resolved luminescence results revealed that the tunable luminescence behavior should be ascribed to the existence of energy migration in the terbium subset, and successive energy transfer process Eu^{2+}-Eu^{3+}(Tb^{3+}) and Tb^{3+}-Eu^{3+} appear to occur in the $Ba_2Tb_{2-y}Si_4O_{13}$:yEu (y = 0-0.12) solid-solution phosphors under investigation.

RSC Advances Accepted Manuscript

1. Introduction

Lanthanide-doped inorganic phosphor materials have attracted much attention in recent years owing to their potential applications in display technology, solid state lighting, and other fields.[1-2] Amongst them, Eu ions have been widely used as activators because both Eu^{3+} and Eu^{2+} can function as emission centers in the host lattices.[3] Comparing with the 4f-5d transition of Eu^{2+}, the emission of the 4f-4f transition of Eu^{3+} is relatively insensitive to the host and temperature because the 4f shell is shielded by the outer filled 5s and 5p shells. However, the 4f-5d transition of Eu^{2+} is parity allowed and therefore intense emission bands can be achieved. In addition, for Eu^{2+} the absorption and emission wavelengths of can be tuned by the host lattice because of the strong interaction between the 5d electron and the ligand anions through covalency and crystal field. Eu^{3+} ions are employed in luminescent devices such as fluorescent lamps and cathode ray tubes, and phosphors containing Eu^{3+} ions as activators can emit red light; their excitation bands usually consist of host lattice excitation bands, charge-transfer bands, and direct excitation bands of Eu^{3+} ions.[4] However, the low oscillator strength and narrow line width of Eu^{3+} 4f-4f absorption transitions leads to a weak absorption in the near-UV and blue region.[5] As a comparison, Eu^{2+} emits in the UV- to visible region and the emission wavelength strongly depends on the nature of the host lattice due to the participation of *d* orbitals. Therefore, as the characteristic broad-band transition excitation and emission of Eu^{2+} have been well recognized, and it might be very exciting and interesting if an efficient Eu^{2+}-Eu^{3+} energy transfer can occur in a single-phase

RSC Advances Accepted Manuscript

valence-varied Eu-doped phosphor, which can provide an opportunity to tailor the absorption of red-emitting phosphors containing Eu^{3+} ions. However, the existence of metal−metal charge transfer (MMCT) effect will quench the luminescence of the sensitizer for the designed Eu^{2+}-Eu^{3+} energy transfer. Therefore, Setlur firstly proposed that energy migration in the terbium subset can be used as an intermediate to alleviate the MMCT effect.[6] After that, such a strategy has been realized in $Ba_3Ln(PO_4)_3$:Ce^{3+},Tb^{3+},Eu^{3+}, $LnPO_4$:Ce^{3+},Tb^{3+},Eu^{3+}, and $Ba_2(Ln_{1-z}Tb_z)(BO_3)_2Cl$:Eu phosphors systems, and some interesting luminescence properties have been observed.[7-8] In the present work, Eu-doped $Ba_2(Gd,Tb)_2Si_4O_{13}$ solid-solution phosphors have been designed, the coexistence of Eu^{2+}/Eu^{3+} has been evidenced and energy transfer of Eu^{2+}-Eu^{3+}(Tb^{3+}) and Tb^{3+}-Eu^{3+} has been observed.

The crystal structures of the $Ba_2Gd_{2-x}Tb_xSi_4O_{13}$ phase under investigation were derived from the $Ba_2Gd_2Si_4O_{13}$ phase via Gd/Tb substitution. $Ba_2Gd_2Si_4O_{13}$ possesses a monoclinic structure and a space group $C2/c$ with lattice parameters a = 12.896(3) Å, b = 5.212(1) Å, c = 17.549(4) Å, β = 104.08(3) Å.[9] Up to now, several studies regarding the luminescence properties of rare earth doped $Ba_2Gd_2Si_4O_{13}$ have been reported. Guo et al. investigated the tunable photoluminescence properties of $Ba_2Gd_2Si_4O_{13}$:Ce^{3+}, Tb^{3+},[10] and the spectroscopic properties of $Ba_2Gd_2Si_4O_{13}$:Eu^{3+}.[11] Zhang et al. studied the vacuum UV spectroscopic properties of $Ba_2Gd_2Si_4O_{13}$:Ln^{3+} (Ln^{3+} = Ce^{3+}, Tb^{3+}, Dy^{3+}, Eu^{3+}, Sm^{3+}).[12] In 2015, Zhou et al. studied the green emitting phosphor $BaGd_2Si_4O_{13}$:Eu^{2+}.[13] Herein, we have investigated the phase formation of $Ba_2(Gd,Tb)_2Si_4O_{13}$, and the coexistence of Eu^{2+}/Eu^{3+}; the energy

RSC Advances Accepted Manuscript

transfer processes Eu^{2+}-Eu^{3+}(Tb^{3+}) and Tb^{3+}-Eu^{3+} in $Ba_2Tb_2Si_4O_{13}$ were investigated in detail.

2. Experimental section

2.1 Sample preparation

$Ba_2Gd_{2-x}Si_4O_{13}$:xTb and $Ba_2Tb_{2-y}Si_4O_{13}$:yEu phosphors were synthesized by high temperature solid-state reaction, starting from a mixture containing commercially-available $BaCO_3$ (99.9%), Gd_2O_3 (99.995%), SiO_2 (99.95%), Tb_4O_7 (99.995%) and Eu_2O_3 (99.995%) in the given stoichiometric proportions. After mixing and grinding, the mixtures were placed into an alumina crucible and then fired in air at 1360 °C for 5 h under a 5%H_2/N_2 gas mixture. After this, the samples were furnace-cooled to room temperature, and ground again into powder for the following measurement.

2.2 Characterization methods

The powder X-ray diffraction (XRD) measurements were conducted on a D8 Advance diffractometer (Bruker Corporation, Germany) operating at 40 kV and 40 mA with Cu Kα radiation (λ = 0.15406 Å), and the scanning rate was fixed at 4^o/min. Diffuse reflectance spectra were measured on a UV-Vis-NIR spectrophotometer (SHIMADZU UV-3600) attached with an integrating sphere. $BaSO_4$ was used as a reference standard. Room temperature photoluminescence (PL) excitation and emission spectra were measured on a fluorescence spectrophotometer (F-4600, HITACHI, Japan) with a photomultiplier tube operating at 400 V, and a 150 W Xe

RSC Advances Accepted Manuscript

lamp used as the excitation lamp. The time-resolved PL spectra were measured by the Edinburgh FLS920 spectrofluorometer with the monitoring wavelength of 377 nm, and the room-temperature decay curves were recorded on the same spectrofluorometer and the corresponding wavelengths (365 nm for Eu^{2+} emission, 377 for Tb^{3+} emission and 393 nm for Eu^{3+} emission) were used to monitor the decay. The temperature-dependence luminescence properties were measured on the same spectrophotometer, which was combined with a self-made heating attachment and a computer-controlled electric furnace. Quantum efficiency was measured using the integrating sphere on the FLS920 fluorescence spectrophotometer (Edinburgh Instruments Ltd., UK).

3. Results and discussion

Fig. 1(a) and Fig. 1(b) show the typical XRD patterns of the as-prepared $Ba_2Gd_{2-x}Si_4O_{13}$:xTb (x = 0, 0.5, 1.0, 1.5, 2.0) and $Ba_2Tb_{2-y}Si_4O_{13}$:yEu (y = 0, 0.01, 0.03, 0.06, 0.15, 2.0) samples, respectively. It can be found that all the diffraction peaks of these two series of samples can be exactly assigned to the corresponding standard data for the hexagonal phase of $Ba_2Gd_2Si_4O_{13}$ (ICSD card no. 260737), indicating that this series of $Ba_2Gd_{2-x}Si_4O_{13}$:xTb (x = 0, 0.5, 1.0, 1.5, 2.0) solid solution samples with different Tb/Gd ratios can form a single phase, and a small amount of Eu also will not change the crystal structure. We find that the characteristic diffraction peak (1 1 4) shifts to higher diffraction angles from 29.28° to 29.40° for $Ba_2Gd_{2-x}Si_4O_{13}$:xTb, while it shifts to lower diffraction angles from 29.40° to 29.22° for $Ba_2Tb_{2-y}Si_4O_{13}$:yEu. This variation could be due to the different ionic radii for Gd^{3+}, Tb^{3+} and Eu^{3+}, further suggesting that continuous solid solution of

RSC Advances Accepted Manuscript

$Ba_2Gd_{2-x}Si_4O_{13}$:xTb and $Ba_2Tb_{2-y}Si_4O_{13}$:yEu have formed in the crystal structure.

The evolution of the unit cell parameters a and V of $Ba_2Gd_{2-x}Si_4O_{13}$:xTb and $Ba_2Tb_{2-y}Si_4O_{13}$:yEu are given in Fig. 2(a) and Fig. 2(b), as a function of x and y, respectively. The linear behavior of the cell parameters illustrate that these two series of compounds both belong to a continuous iso-structural solid solution. Fig. 2(c) presents the crystal structure of $Ba_2(Gd,Tb)_2Si_4O_{13}$. The structure is based on finite zigzag-shaped C_2-symmetric Si_4O_{13} chains and Gd_2O_{12} dimers built of edge-sharing GdO_7 polyhedra of C_1 symmetry. The [9+1]-coordinated Ba atoms are located in voids of the atomic arrangement, as highlighted in Fig. 2(d).

Room temperature photoluminescence excitation (PLE) and emission (PL) spectra of the $Ba_2Gd_{1.99}Si_4O_{13}$:0.01Eu phosphors are shown in Fig. 3(a). Upon excitation at 365 nm, the PL spectra of $Ba_2Gd_{1.99}Si_4O_{13}$:0.01Eu presents a broad band in the green region (350-600 nm) and several small peaks on the shoulders near 600 nm. It is well known that Eu^{2+} ions provide a broad emission band corresponding to the $4f^65d$-$4f^7$ transition, while Eu^{3+} ions emit discrete narrow lines belonging to the $^5D_0$-^7F_J transitions (J = 0-6). Moreover, the two excitation spectra for $Ba_2Gd_{1.99}Si_4O_{13}$:0.01Eu give the corresponding typical spectral profile for the two ions. Although the europium precursor was Eu_2O_3 containing the trivalent ion and the samples were prepared in a reducing atmosphere, it seems that the trivalent europium coexists with divalent europium in this compound. In order to prove it, a Eu^{3+} singly doped $Ba_2Gd_2Si_4O_{13}$ phosphor was prepared in air and its PLE and PL spectra were comparatively investigated. As also shown in Fig. 3(a), there are three

RSC Advances Accepted Manuscript

narrow peaks centered at 594, 613 and 624 nm in the PL spectrum of $Ba_2Gd_{1.99}Si_4O_{13}:0.01Eu^{3+}$ upon 393 nm excitation, which agrees with the position of Eu^{3+} emission in $Ba_2Gd_{1.99}Si_4O_{13}:0.01Eu^{2+}/Eu^{3+}$. Furthermore, the PLE spectral profile of $Ba_2Gd_{1.99}Si_4O_{13}:0.01Eu^{3+}$ is similar to that of $Ba_2Gd_{1.99}Si_4O_{13}:0.01Eu^{2+}/Eu^{3+}$ monitored at 613 nm; this confirms the consistence of Eu^{2+} and Eu^{3+} in the $Ba_2Gd_2Si_4O_{13}$ host when prepared in reducing atmosphere. Fig. 3(b) shows the PLE (λ_{em} = 543 nm) and PL (λ_{em} = 377 nm) spectra of $Ba_2Gd_{1.99}Si_4O_{13}:0.01Tb^{3+}$. The PLE spectrum observed in the range of 200-300 nm were attributed to the $4f^8$- $4f^75d^1$ ($^7F_6$-^7D) transition of Tb^{3+} and those in the range of 300-400 nm were come from the 4f-4f transition of Tb^{3+}. The Tb^{3+} emission lines are located at 487 nm, 542 nm, 585 nm, and 624 nm, and are assigned to the $^5D_4$ -$^7F_{6, 5, 4, 3}$ transitions, respectively.[14]

The decay curves and lifetime values of Eu^{2+}/Eu^{3+} (excitation wavelength 365 nm for Eu^{2+} and 393 nm for Eu^{3+}) and Tb^{3+} (excitation wavelength 377 nm) in $Ba_2Gd_{1.99}Si_4O_{13}:0.01Eu/Tb$ phosphor are shown in Fig. 4. Since there are several different cations with variable environments for the doped rare earth ions in this system, we have tried different exponential functions. It is found that, in order to get the best fitting (with the confidence coefficient of 99%) and evaluate the decay time, the experimental curves were fitted by the sum of two exponential decays using the formula:[15]

$$I(t) = A_1 \exp(-t/\tau_1) + A_2 \exp(-t/\tau_2) \quad (1)$$

where I is the luminescence intensity, A_1 and A_2 are constants, τ is the time, τ_1 and τ_2

RSC Advances Accepted Manuscript

are rapid and slow lifetimes for exponential components, respectively. On this basis, the effective lifetime constant (τ^*) can be calculated as:[16]

$$\tau^* = \left(A_1\tau_1^{\ 2} + A_2\tau_2^{\ 2}\right)/\left(A_1\tau_1 + A_2\tau_2\right) \quad (2)$$

The effective decay time (τ^*) were calculated to be 2.01 μs, 1.96 ms, 1.89 ms and 2.21 ms for the $4f^65d$-$4f^7$ (Eu^{2+} emission at 507 nm) in $Ba_2Gd_{1.99}Si_4O_{13}$:0.01Eu, $^5D_0$-$^7F_2$ (Eu^{3+} emission at 613 nm) in $Ba_2Gd_{1.99}Si_4O_{13}$:0.01Eu, $^5D_0$-$^7F_2$ (Eu^{3+} emission at 613 nm) in $Ba_2Gd_{1.99}Si_4O_{13}$:0.01Eu^{3+}, and $^5D_4$-$^7F_5$ (Tb^{3+} emission at 543 nm) in $Ba_2Gd_{1.99}Si_4O_{13}$:0.01Tb^{3+}, respectively. The decay profile of the $^5D_4$ emission for the latter sample shows a clear rise at short times, due to the slow relaxation from $^5D_3$ to $^5D_4$, attributed to multiphonon relaxation in the silicate host containing high frequency vibrations. The non-exponential character of the decay profiles is presumably due to the presence of several slightly different sites for the dopants and, in the case of $Ba_2Gd_{1.99}Si_4O_{13}$:0.01Eu, to possible Eu^{2+}-Eu^{3+} energy transfer processes.

The possibility of the Eu^{2+}/Eu^{3+} coexistence can be verified by the luminescence behavior. Fig. 5(a) shows the PLE and PL spectra of $Ba_2Tb_2Si_4O_{13}$. It can be seen that the PLE spectrum of Tb^{3+} exhibits two obvious broad bands from 200 to 300 nm with two peaks at 252 and 279 nm and some weak transitions from 300 to 400 nm. Fig. 5(b) represents the PLE and PL spectra of $Ba_2Tb_{1.97}Si_4O_{13}$:0.03Eu obtained at different experimental conditions. When Eu ions with a low concentration (y = 0.03) were introduced into this matrix, the PLE spectrum of $Ba_2Tb_{1.97}Si_4O_{13}$:0.03Eu phosphor prepared in reducing atmosphere has been obviously broadened and the intensity of the sharp lines corresponding to the emission of Tb^{3+} has obviously increased.

RSC Advances Accepted Manuscript

Moreover, the excitation band edge has shifted to 450 nm, showing a broad-band character. By comparing the two excitation bands of $Ba_2Tb_{1.97}Si_4O_{13}$:0.03Eu phosphor obtained at different experimental conditions, there is an obvious difference in the excitation band owing to the appearance of a broad excitation band, which supports the existence of Eu^{2+}. Upon excitation at 377 nm, the Tb^{3+} emission intensity decreases accompanied by a remarkable increase of the emission intensities at 594, 613, and 624 nm for $Ba_2Tb_{1.97}Si_4O_{13}$:0.03Eu phosphor, which are the characteristic red emission peaks of Eu^{3+} ions corresponding to the transitions from $^5D_0$ to ^7F_J (J = 1 and 2).[17] Generally, we can propose that the enhancement of the red-emitting luminescence can be ascribed to the energy transfer from Tb^{3+} to Eu^{3+}.[18-19] Furthermore, it is notable that the emission intensity of the $Ba_2Tb_{1.97}Si_4O_{13}$:0.03Eu phosphor prepared in reducing atmosphere is relatively higher than the one of the $Ba_2Tb_{1.97}Si_4O_{13}$:0.03Eu fired in air, indicating that the efficient energy transfer between Eu^{2+}-Eu^{3+} (Tb^{3+}) and the Eu^{2+} absorption.

The diffuse reflectance spectra of $Ba_2Gd_{2-x}Si_4O_{13}$:xTb (x = 0, 0.5, 1.0, 1.5, 2.0) phosphors are shown in Fig. 6(a). The spectrum of the $Ba_2Gd_2Si_4O_{13}$ host shows a high reflectance in the visible range, and the band gap estimation in the $Ba_2Gd_2Si_4O_{13}$ host is shown by the inset in Fig. 6(a). The band gap of the $Ba_2Gd_2Si_4O_{13}$ host can be estimated according to eq 3[20]

$$\left[F(R_\infty)h\nu\right]^n = A\left(h\nu - E_g\right) \quad (3)$$

where $h\nu$ is the photon energy; A is a proportional constant; E_g is the value of the band gap; n = 2 for a direct transition or 1/2 for an indirect transition; and $F(R_\infty)$ is

RSC Advances Accepted Manuscript

the Kubelka-Munk function defined as[21]

$$F(R_\infty) = (1 - R)^2 / 2R = K/S \quad (4)$$

where R, K, and S are the reflection, absorption, and scattering coefficient, respectively. From the linear extrapolation of $[F(R_\infty)h\nu]^2 = 0$ in the inset of Figure 6a, the E_g value was estimated to be about 4.20eV. As Tb^{3+} ions were doped into the $Ba_2Gd_2Si_4O_{13}$ host, a strong absorption in the range of 200-350 nm assigned to the the f-d transition of Tb^{3+} was observed, as found in the excitation spectrum. The E_g value gradually increases, and the absorption intensity is enhanced at higher Tb^{3+} ion concentrations. As a comparison, $Ba_2Tb_{2-y}Si_4O_{13}$:yEu phosphors show an obvious broad absorption band near 400 nm (Fig. 6(b)), which should be caused by the $4f^7$-$4f^6 5d^1$ transition of Eu^{2+}.[22] The reflectance spectrum and PLE spectrum indicate that the absorption of $Ba_2Tb_2Si_4O_{13}$:Eu phosphor matches well with near-UV chips for applications in near-UV LEDs.

Fig. 7(a) illustrates the emission spectra of $Ba_2Tb_{2-y}Si_4O_{13}$:yEu (y = 0-0.12) samples upon excitation at 377 nm. With increasing Eu concentration, one can see that the relative emission intensities of Tb^{3+} becomes weak, whereas the emission intensities of Eu^{3+} firstly increase until they reach saturation at y = 0.03, reflecting the result of energy transfer from Tb^{3+} to Eu^{3+}. In addition, it is surprising to find the appearance of a broad band centered around 507 nm with increasing y, which can be assigned to the $4f^6 5d^1$-$4f^7$ transition of Eu^{2+}, further supporting the coexistence of Eu^{2+} and Eu^{3+}.[23] Because of the Eu^{2+}-$(Tb^{3+})_n$-Eu^{3+} energy transfer process, the CIE coordinates upon 377 nm excitation of $Ba_2Tb_{2-y}Si_4O_{13}$:yEu (y = 0, 0.01, 0.03, 0.09)

RSC Advances Accepted Manuscript

progressively shifted from green (0.2966, 0.5798) to red (0.5048, 0.3955) with increasing *y* as displayed in Fig. 7(b). As also given in the photographs of the emitting phosphors, the as-observed emitting color is obvious, which means that the tunable luminescence can be realized in the novel $Ba_2Tb_{2-y}Si_4O_{13}$:*y*Eu phosphors via Eu^{2+}-$(Tb^{3+})_n$-Eu^{3+} energy transfer processes.

In order to demonstrate the energy transfer from Tb^{3+} to Eu^{3+}, the decay curves of Tb^{3+} emission at 542 nm and Eu^{3+} emission at 613 nm of $Ba_2Tb_2Si_4O_{13}$ and $Ba_2Tb_{1.995}Si_4O_{13}$:0.005Eu phosphors are shown in Fig. 8(a) (Excitation at 377 nm). Using Eq 1 and Eq 2, the values of the effective decay time were found to be 2.59, 0.96 and 1.83 ms for the $^5D_4$-$^7F_5$ (Tb^{3+} emission at 543 nm) in $Ba_2Tb_2Si_4O_{13}$, $^5D_4$-$^7F_5$ (Tb^{3+} emission at 543 nm) in $Ba_2Tb_{1.995}Si_4O_{13}$:0.005Eu, and $^5D_0$-$^7F_2$ (Eu^{3+} emission at 613 nm) in $Ba_2Tb_{1.995}Si_4O_{13}$:0.005Eu, respectively. Accordingly, the energy transfer efficiency (η_T) can be calculated using the following expression:[24]

$$\eta_T = 1 - \frac{\tau_x}{\tau_0} \quad (5)$$

here τ_0 and τ_x are the corresponding lifetime values of donor Tb^{3+} in the absence and the presence of the acceptor Eu^{3+}, and η_T is the energy transfer efficiency. As shown in the inset of Fig. 8(a), the total η_T is found to be 62.9% from Tb^{3+} to Eu^{3+} in the $Ba_2Tb_{1.995}Si_4O_{13}$:0.005Eu phosphor. We also measured the decay curves of the $Ba_2Tb_{2-y}Si_4O_{13}$:*y*Eu phosphors excited at 377 nm, as given in Fig. 8(b). It was found that the lifetimes for Tb^{3+} decreased with increasing Eu concentraion, which offers clear evidence for the presence of energy transfer from Tb^{3+} to Eu^{3+}, and the energy transfer efficiencies are 62.9%, 68.7%, 73.7%, 81.5% and 89.2% depending on

RSC Advances Accepted Manuscript

different Eu concentration, 0.005, 0.01, 0.02, 0.03 and 0.06, respectively. Fig. 8(c) shows the decay curves of the $^5D_4$-$^7F_5$ transition of Tb^{3+} upon excitation at 273, 365, and 377 nm. Based on the decay curves in Fig. 8(c), Eq 1 and Eq 2, the value of decay time were calculated to be practically independent of the excitation wavelength, with values 0.49, 0.45 and 0.48 ms for excitation of 273, 365, and 377 nm, respectively.

To study the energy transfer process from Tb^{3+} to Eu^{3+} in $Ba_2TbSi_4O_{13}$:Eu phosphor in more detail, time-resolved emission spectra of $Ba_2Tb_{1.995}Si_4O_{13}$:0.005Eu were measured upon excitation into the Tb^{3+} band with a delay time ranging from 0 to 3.12 ms (Fig. 9). At t = 0 ms, only the characteristic emission Tb^{3+} is observed; no Eu^{3+} emission is present because the excitation energy Tb^{3+} has not been transferred yet to Eu^{3+}. As also shown in Fig. 9, when t = 0.78 ms, the emission of Tb^{3+} starts to decrease accompanied by the presence of Eu^{3+} emissions due to the efficient energy transfer of Tb^{3+} to Eu^{3+}. The emission of Tb^{3+} decreases gradually with further increase of the decay time, whereas that of Eu^{3+} begins to increase due to transfer of more excitation energy from Tb^{3+} to Eu^{3+}. Therefore, the Eu^{3+} ion acts as the terminal of the thermal of the energy transfer processes in the $Ba_2TbSi_4O_{13}$:Eu phosphor. Thus, we can obtain bright red luminescence in the $Ba_2TbSi_4O_{13}$:Eu phosphor upon near UV excitation.

Fig. 10 illustrates the energy level model for the energy transfer processes of and Eu^{2+}-Tb^{3+}-Eu^{3+} in the $Ba_2Tb_2Si_4O_{13}$ host. As can be seen from Fig. 10, the excitation lines of $Ba_2Tb_2Si_4O_{13}$:Eu phosphors in the *n*-UV region come from the

RSC Advances Accepted Manuscript

absorption of the combined effect of Tb^{3+}, Eu^{3+}, and Eu^{2+}, so that a broad and strong absorption band can be observed in the PLE spectrum (Figure 3b). The energy absorbed by Eu^{2+} can also be efficiently transferred from the $4f^6 5d^1$ band to the excited levels of Eu^{3+} and Tb^{3+}; accordingly, the energy absorbed by Tb^{3+} can be transferred from the $^5D_4$ level of Tb^{3+} to the $^5D_0$ ($^5D_1$) level of Eu^{3+}.[25-26]

The thermal stability of phosphor is one of the important parameters for possible applications. For this reason, the emission spectra of the selected $Ba_2Tb_{1.97}Si_4O_{13}$:0.03Eu phosphor at various temperatures are shown in Fig. 11(a). The variations of the relative emission intensities as a function of temperature are plotted in Fig. 11(b). When the temperature is increased to 150 ^oC, the PL intensities of Tb^{3+} and Eu^{3+} ions decrease to 94.9% and 88.2% of the corresponding initial value (25 ^oC). In Fig. 11(b), we have also given the temperature dependent PL intensities variation of the commercial $BaMgAl_{10}O_{19}:Eu^{2+}$ (BAM) blue phosphor, and the comparable thermal stability can be found. The small intensity decrease indicates that $Ba_2Tb_2Si_4O_{13}$:Eu could be used for high-power LED application. In general, the thermal quenching of emission intensity can be explained by several mechanisms. A widely accepted mechanism is the electronic transition through the intersection between the ground and excited states. In other words this mechanism is described as a large displacement between the potential energy curves of the ground and excited state in the configuration coordinate diagram.[27] In the present case, this mechanism would be valid in the case of excitation in the absorption profile of Eu^{2+}. To better understand the thermal quenching phenomena, the activation energy for the thermal

RSC Advances Accepted Manuscript

quenching was fitted using the equation describing the crossover between Franck Condon displaced potential energy curves:[28-29]

$$I_T = \frac{I_0}{1 + c\exp(-\frac{\Delta E}{kT})} \quad (6)$$

where I_0 is the initial PL intensity of the phosphor at room temperature, I_T is the PL intensity at different temperatures, c is a constant, ΔE is the activation energy for thermal quenching, and k is Boltzmann constant (8.62×10^{-5}eV). According to the equation, the activation energy ΔE can be calculated from a plotting of $\ln[(I_0/I)-1]$ against $1/kT$, where a straight slope equals $-\Delta E$. As shown in Fig. 11(b), ΔE were found to be 0.351 and 0.296 eV for Tb^{3+} and Eu^{3+}, respectively. The relatively high activation energy results in a good thermal stability for this phosphor. The quantum efficiency of the phosphor is another important parameter to be considered for practical application, and we have also measured the internal quantum efficiency (QE) of $Ba_2Tb_{2-x}Si_4O_{13}$:xEu (x = 0, 0.005, 0.03 and 0.09) phosphors. The measured internal QE values are 30.06%, 31.66%, 39.35% and 23.39%, respectively, for x = 0, 0.005, 0.03, 0.09 under 377 nm excitation.

4. Conclusion

In summary, color-tunable $Ba_2Gd_{2-x}Tb_xSi_4O_{13}$:$y$Eu solid-solution phosphors were prepared by the high-temperature solid-state reaction in reducing atmosphere. The terbium ions in the host can not only form the iso-structural phase originated from the $Ba_2Gd_2Si_4O_{13}$, but they can be also used to realize the Eu^{2+}-$(Tb^{3+})_n$-Eu^{3+} energy transfer channel between broad-band absorption of Eu^{2+} and the narrow-line emission of Eu^{3+}. On the basis of this process, the emission color of the obtained

RSC Advances Accepted Manuscript

phosphors can be varied from green to yellow and finally to red by adjusting the concentration of Eu. Moreover, the temperature dependence of the luminescence intensity shows that this phosphor has an excellent thermal stability against temperature quenching.

Acknowledgements

The present work was supported by the National Natural Science Foundations of China (Grant No. No.51572023, No.51272242), Natural Science Foundations of Beijing (2132050), the Program for New Century Excellent Talents in University of Ministry of Education of China (NCET-12-0950), Beijing Nova Program (Z131103000413047), Beijing Youth Excellent Talent Program (YETP0635), the Funds of the State Key Laboratory of New Ceramics and Fine Processing, Tsinghua University (KF201306), and Fundamental Research Funds for the Central Universities (FRF-TP-15-005A2).

References

1 J. C. Bünzli, *Nat. Chem.,* 2010, **2**, 698.

2 G. G. Zhang, J. Wang, Y. Chen and Q. Su, *Opt. Lett.,* 2010, **35**, 2382.

3 G. J. Gao, S. Reibstein, M. Y. Peng and L. Wondraczek, *J. Mater. Chem.,* 2011, **21**, 3156.

4 M. Y. Peng, Z. W. Pei, G. Y. Hong and Q. Su, *J. Mater. Chem.,* 2003, **13**, 1202.

5 K. H. Kwon, W. B. Im, H. S. Jang, H. S. Yoo and D. Y. Jeon, *Inorg. Chem.,* 2009**, 48**, 11525.

6 A. A. Setlur, *Electrochem. Solid-State Lett.,* 2012, **15**, J25.

RSC Advances Accepted Manuscript

7 D. W. Wen, J. X. Shi, M. M. Wu and Q. Su, *ACS Appl. Mater. Interfaces.,* 2014**, 6**, 10792.

8 Z. G. Xia, J. Q. Zhuang, A. Meijerink and X. P, Jing, *Dalton. Trans.,* 2013**, 42**, 6327.

9 M. Wierzbicka-Wieczorek, U. Kolitsch and E. Tillmanns, *Acta Cryst. C,* 2010**, 66**, 129.

10 H. Guo, H. Zhang, J. J. Li and F. Li, *Opt. Express.,* 2010**, 18**, 27257.

11 H. Guo, H. Zhang, R. F. Wei, M. D. Zheng and L. H. Zhang, *Opt. Express.,* 2011**, 19**, A201.

12 F. Zhang, Y. Wang and Y. Tao, *Mater. Res. Bull.,* 2013**, 48**, 1952.

13 H. P. Zhou, Q. P. Wang, M. S. Jiang, X. X. Jiang and Y. Jin, *Dalton. Trans.,* 2015, **44**, 13962.

14 E. Zych, J. Trojan-Piegza, D. Hreniak and W. Strek, *J. Appl. Phys.,* 2003, **94**, 1318.

15 P. L. Li, Z. J. Wang, Z. P. Yang and Q. L. Guo, *Opt. Commun.,* 2014, **332**, 83.

16 P. I. Paulose, G. Jose, V. Thomas, N. V. Unnikrishnan and M. K. R. Warrier, *J. Phys. Chem. Solids.,* 2003, **64**, 841.

17 J. Yang, C. M. Zhang, C. X. Li and J. Lin, *Inorg. Chem.,* 2008, **47**, 7262.

18 F. H. Le, L. X. Wang, W. Jia, D. Z. Jia and S. J. Bao, *J. Alloys. Compd.,* 2012, **512**, 323.

19 T. Li, P. L. Li, Z. J. Wang, S. C. Xu, Q. Y. Bai and Z. P. Yang, *Dalton. Trans.,* 2015, **44**, 16840.

20 J. Wang, S. B. Wang and Q. Su, *J. Solid. State. Chem.,* 2004, **177**, 895.

21 Z. G. Xia, Y. Y. Zhang, M. S. Molokeev and V. V. Atuchin, *J. Phys. Chem. C,* 2013, **117**, 20847.

RSC Advances Accepted Manuscript

22 W. B. Im, N. N. Fellows, S. P. Denbaars, R. Seshadri and Y. Kim, *Chem. Mater.,* 2009, **21**, 2957.

23 Y. Zhang, X. J. Li, K. Li, H. Z. Lian, M. M. Shang and J. Lin, *ACS Appl. Mater. Inter.,* 2015, **7**, 2715.

24 Z. G. Xia and R. S. Liu, *J. Phys. Chem. C,* 2012, **116**, 15604.

25 M. Bettinelli and C. D. Flint, *J. Phys.: Condens. Matter.,* 1990, **2**, 8417.

26 S. C. Xu, P. L. Li, Z. J. Wang, T. Li, Q. Y. Bai, J. Sun and Z. P. Yang, *J. Mater. Matter. C,* 2015, **3**, 9112.

27 H. D. Luo, J. Liu, X. Zheng, L. X. Han, K. X. Ren and X. B. Yu, *J. Mater. Chem.* 2012, **22**, 15887.

28 J. Zhou and Z. G. Xia, *Sci. Rep*., 2015, **3**, 12149.

29 W. H, Fonger and C. W. Struck, *J. Chem. Phys.,* 1970, **52**, 6364.

RSC Advances Accepted Manuscript

The figure captions are as follows,

Fig. 1 XRD patterns of as-prepared (a) $Ba_2Gd_{2-x}Si_4O_{13}$:xTb (x = 0, 0.5, 1.0, 1.5, 2.0) and (b) $Ba_2Tb_{2-y}Si_4O_{13}$:yEu (y = 0, 0.01, 0.03, 0.06, 0.15, 2.0) samples. The standard data for $Ba_2Gd_2Si_4O_{13}$ (ICSD card no. 260737) is shown as a reference.

Fig. 2 Unit cell parameters a, V of (a) $Ba_2Gd_{2-x}Si_4O_{13}$:xTb (x = 0, 0.5, 1.0, 1.5, 2.0) and (b) $Ba_2Tb_{2-y}Si_4O_{13}$:yEu (y = 0, 0.01, 0.03, 0.06, 0.15)are plotted. (c) Crystal structure of $Ba_2Gd_2Si_4O_{13}$ viewed along the b axis. The SiO_4 tetrahedra and GdO_7 polyhetra are highlighted in the unit cell, and $Ba_2Tb_2Si_4O_{13}$ is isostructural with $Ba_2Gd_2Si_4O_{13}$. (d) The bonding of O^{2-} anions with Ba^{2+}, Si^{4+} and Gd^{3+} cations in the independent part of the $Ba_2(Gd,Tb)_2Si_4O_{13}$ unit cell.

Fig. 3 PLE and PL spectra of (a) $Ba_2Gd_{1.99}Si_4O_{13}$:0.01Eu^{2+}/Eu^{3+} prepared in a reducing atmosphere, $Ba_2Gd_{1.99}Si_4O_{13}$:0.01Eu^{3+} prepared in air, and (b) $Ba_2Gd_{1.99}Si_4O_{13}$:0.01Tb^{3+} prepared in air.

Fig. 4 (a) Decay time curves and the corresponding lifetime values of Eu^{2+} in $Ba_2Gd_{1.99}Si_4O_{13}$:0.01Eu phosphor. (b) Eu^{3+} and Tb^{3+} decay curves of $Ba_2Gd_{1.99}Si_4O_{13}$:0.01Eu/Tb phosphor.

Fig. 5 PLE and PL spectra of (a) $Ba_2Tb_2Si_4O_{13}$ and (b) $Ba_2Tb_{1.97}Si_4O_{13}$:0.03Eu phosphor.

Fig. 6 The diffuse reflectance spectra of (a) $Ba_2Gd_{2-x}Si_4O_{13}$:xTb (x = 0, 0.5, 1.0, 1.5, 2.0) and (b) $Ba_2Tb_{2-y}Si_4O_{13}$:yEu (y = 0, 0.01, 0.04, 0.06) phosphors. The extrapolation of the band gap energy for (inset of a) $Ba_2Gd_2Si_4O_{13}$, (inset of b) $Ba_2Tb_2Si_4O_{13}$, (c) $Ba_2Gd_{1.5}Tb_{0.5}Si_4O_{13}$, (d) $Ba_2GdTbSi_4O_{13}$, and (e)

RSC Advances Accepted Manuscript

$Ba_2Gd_{0.5}Tb_{1.5}Si_4O_{13}$.

Fig. 7 (a) PL spectra for the phosphors $Ba_2Tb_{2-y}Si_4O_{13}$:yEu (y = 0, 0.005, 0.01, 0.03, 0.04, 0.06, 0.09, 0.12) phosphors, and (b) the corresponding CIE coordinates and pihotographs.

Fig. 8 (a) Decay time curves and lifetimes of Eu^{3+} in $Ba_2Tb_{1.995}Si_4O_{13}$:0.005Eu phosphor and Tb^{3+} in $Ba_2Tb_2Si_4O_{13}$ and $Ba_2Tb_{1.995}Si_4O_{13}$:0.005Eu phosphor. (b) Tb^{3+} decay curves of $Ba_2Tb_{2-y}Si_4O_{13}$:yEu phosphors monitoring 542 nm emission. (c) Tb^{3+} decay curves of $Ba_2Tb_{1.97}Si_4O_{13}$:0.03Eu phosphors monitoring 542 nm emission under 273, 365 and 377 nm excitation.

Fig. 9 The time-resolved spectra of $Ba_2Tb_{1.995}Si_4O_{13}$:0.005Eu phosphor under 377 nm excitation.

Fig. 10 Energy level diagram for the ET processes among Eu^{2+}, Tb^{3+}, and Eu^{3+} in $Ba_2Tb_2Si_4O_{13}$ phosphor.

Fig. 11 (a) Temperature-dependent PL spectra of $Ba_2Tb_{1.97}Si_4O_{13}$:0.03Eu. (b) The variations of the relative emission intensities as a function of temperature of the $Ba_2Tb_{1.97}Si_4O_{13}$:0.03Eu phosphor and commercial BAM phosphor. The inset shows relative PL intensities of Tb^{3+}, and Eu^{3+} in $Ba_2Tb_2Si_4O_{13}$ host with raised temperatures. The inset shows the activation energy (ΔE) of Tb^{3+} and Eu^{3+} in $Ba_2Tb_{1.97}Si_4O_{13}$:0.03Eu phosphor.

RSC Advances Accepted Manuscript

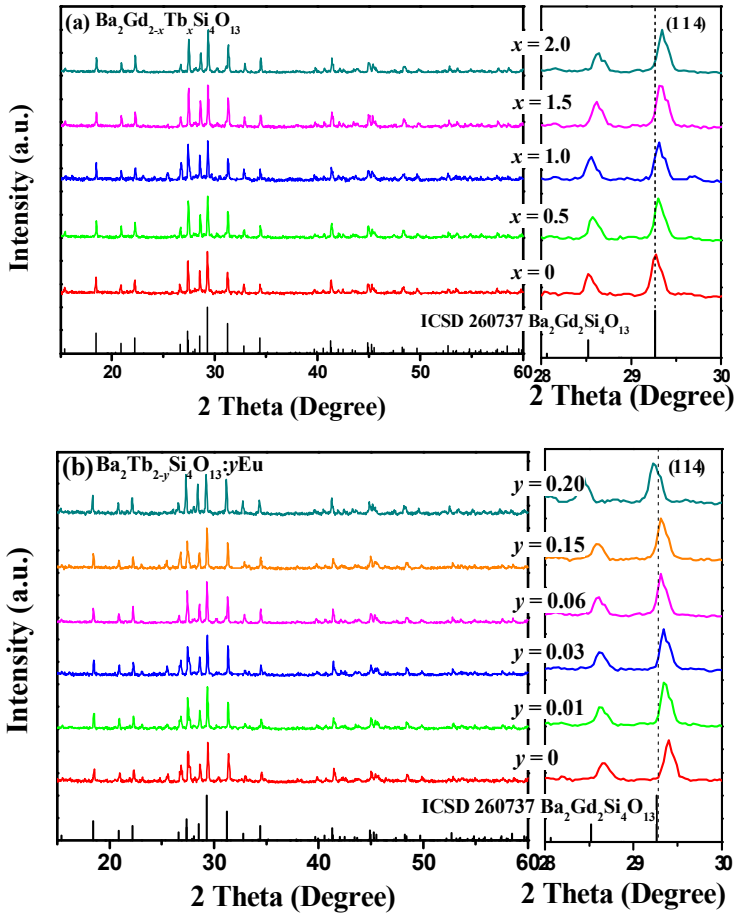

Fig. 1 XRD patterns of as-prepared (a) $Ba_2Gd_{2-x}Si_4O_{13}$:xTb (x = 0, 0.5, 1.0, 1.5, 2.0) and (b) $Ba_2Tb_{2-y}Si_4O_{13}$:yEu (y = 0, 0.01, 0.03, 0.06, 0.15, 2.0) samples. The standard data for $Ba_2Gd_2Si_4O_{13}$ (ICSD card no. 260737) is shown as a reference.

RSC Advances Accepted Manuscript

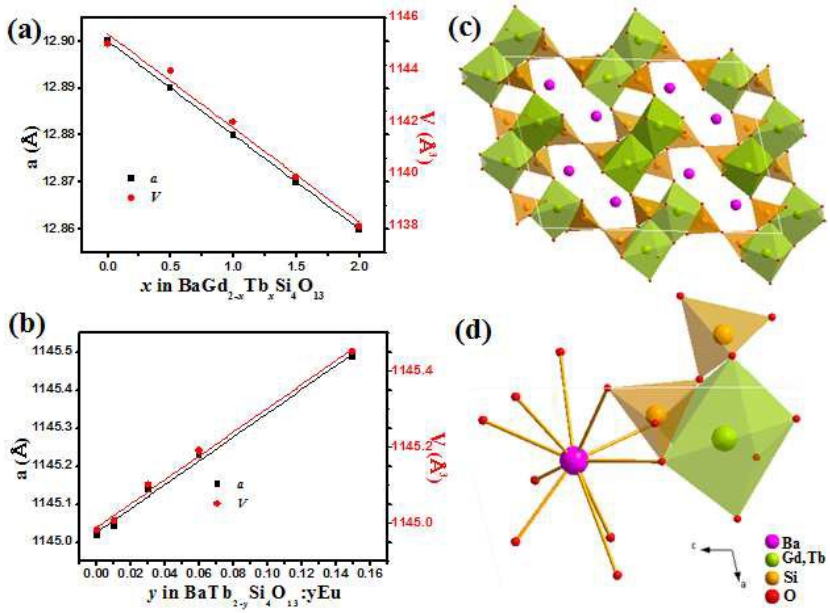

Fig. 2 Unit cell parameters *a*, *V* of (a) $Ba_2Gd_{2-x}Si_4O_{13}$:*x*Tb (*x* = 0, 0.5, 1.0, 1.5, 2.0) and (b) $Ba_2Tb_{2-y}Si_4O_{13}$:*y*Eu (*y* = 0, 0.01, 0.03, 0.06, 0.15)are plotted. (c) Crystal structure of $Ba_2Gd_2Si_4O_{13}$ viewed along the *b* axis. The SiO_4 tetrahedra and GdO_7 polyhetra are highlighted in the unit cell, and $Ba_2Tb_2Si_4O_{13}$ is isostructural with $Ba_2Gd_2Si_4O_{13}$. (d) The bonding of O^{2-} anions with Ba^{2+}, Si^{4+} and Gd^{3+} cations in the independent part of the $Ba_2(Gd,Tb)_2Si_4O_{13}$ unit cell.

RSC Advances Accepted Manuscript

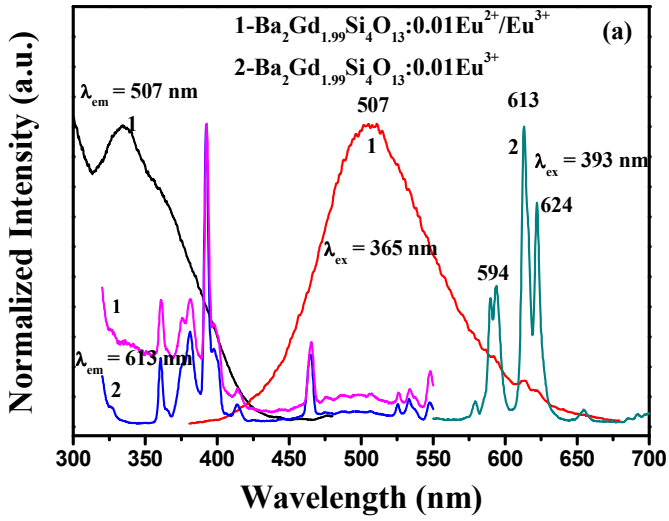

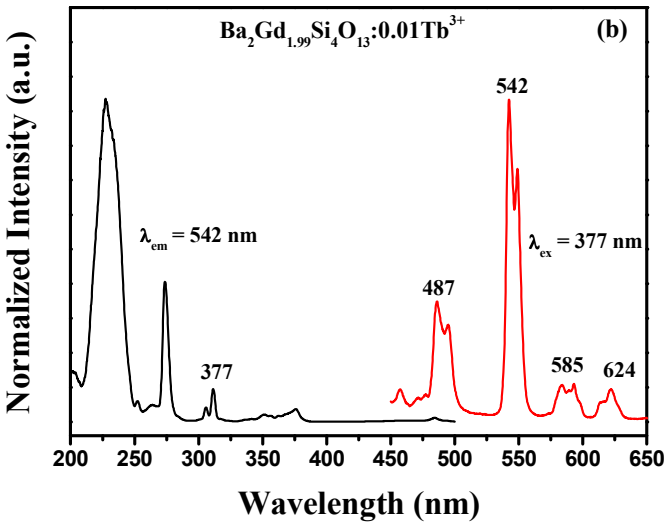

Fig. 3 PLE and PL spectra of (a) $Ba_2Gd_{1.99}Si_4O_{13}:0.01Eu^{2+}/Eu^{3+}$ prepared in a reducing atmosphere, $Ba_2Gd_{1.99}Si_4O_{13}:0.01Eu^{3+}$ prepared in air, and (b) $Ba_2Gd_{1.99}Si_4O_{13}:0.01Tb^{3+}$ prepared in air.

RSC Advances Accepted Manuscript

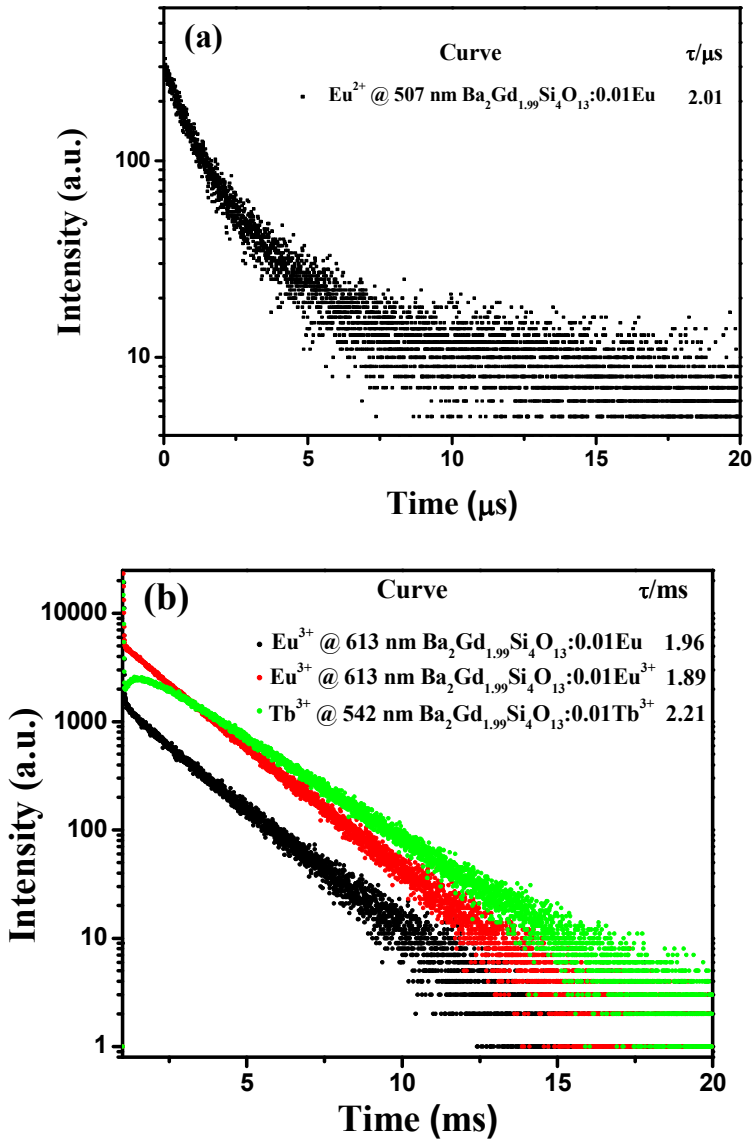

Fig. 4 (a) Decay time curves and the corresponding lifetime values of Eu^{2+} in $Ba_2Gd_{1.99}Si_4O_{13}$:0.01Eu phosphor. (b) Eu^{3+} and Tb^{3+} decay curves of $Ba_2Gd_{1.99}Si_4O_{13}$:0.01Eu/Tb phosphor.

RSC Advances Accepted Manuscript

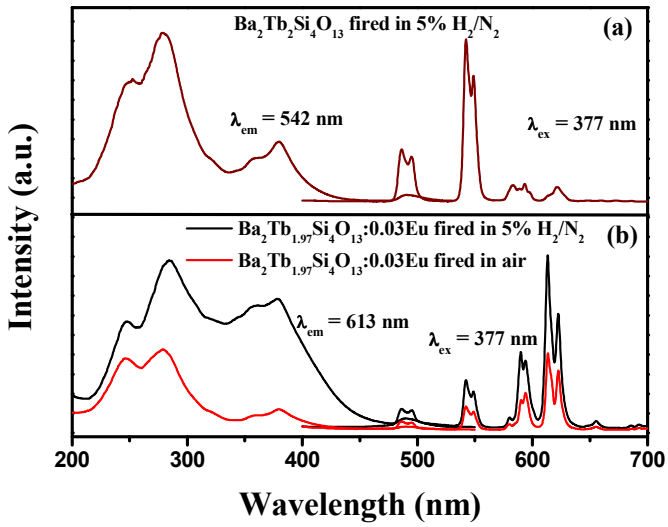

Fig. 5 PLE and PL spectra of (a) $Ba_2Tb_2Si_4O_{13}$ and (b) $Ba_2Tb_{1.97}Si_4O_{13}$:0.03Eu phosphor.

RSC Advances Accepted Manuscript

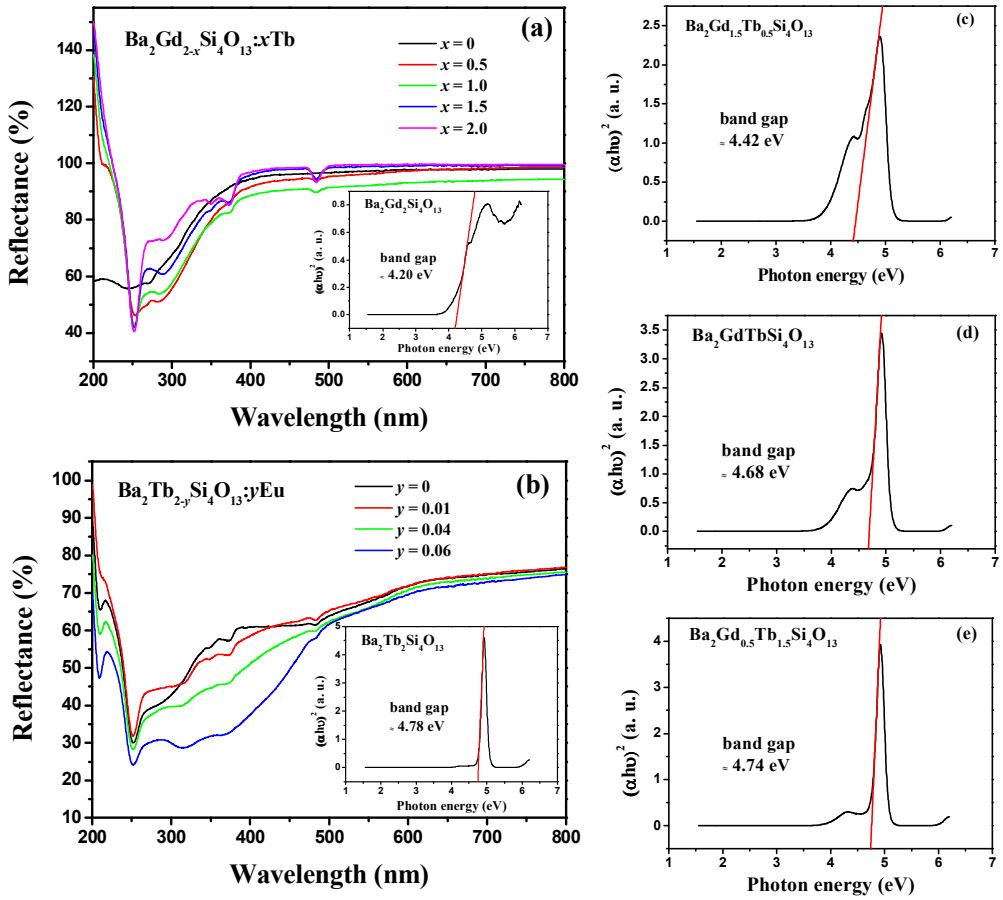

Fig. 6 The diffuse reflectance spectra of (a) $Ba_2Gd_{2-x}Si_4O_{13}$:xTb (x = 0, 0.5, 1.0, 1.5, 2.0) and (b) $Ba_2Tb_{2-y}Si_4O_{13}$:yEu (y = 0, 0.01, 0.04, 0.06) phosphors. The extrapolation of the band gap energy for (inset of a) $Ba_2Gd_2Si_4O_{13}$, (inset of b) $Ba_2Tb_2Si_4O_{13}$, (c) $Ba_2Gd_{1.5}Tb_{0.5}Si_4O_{13}$, (d) $Ba_2GdTbSi_4O_{13}$, and (e) $Ba_2Gd_{0.5}Tb_{1.5}Si_4O_{13}$.

RSC Advances Accepted Manuscript

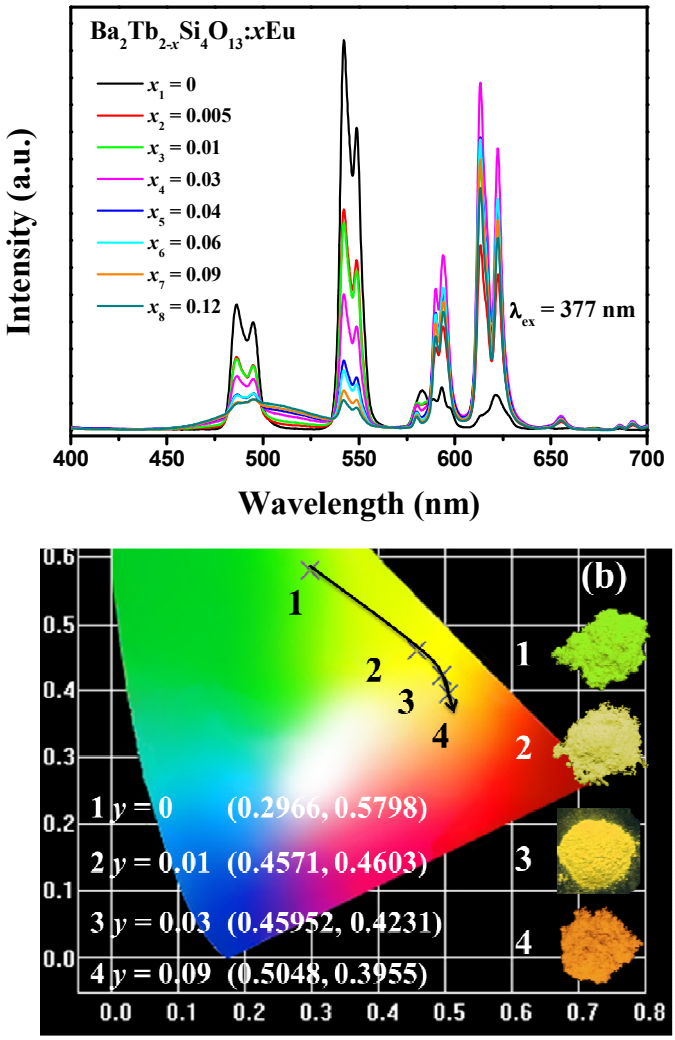

Fig. 7 (a) PL spectra for the phosphors $Ba_2Tb_{2-y}Si_4O_{13}$:yEu (y = 0, 0.005, 0.01, 0.03, 0.04, 0.06, 0.09, 0.12) phosphors, and (b) the corresponding CIE coordinates and photographs.

RSC Advances Accepted Manuscript

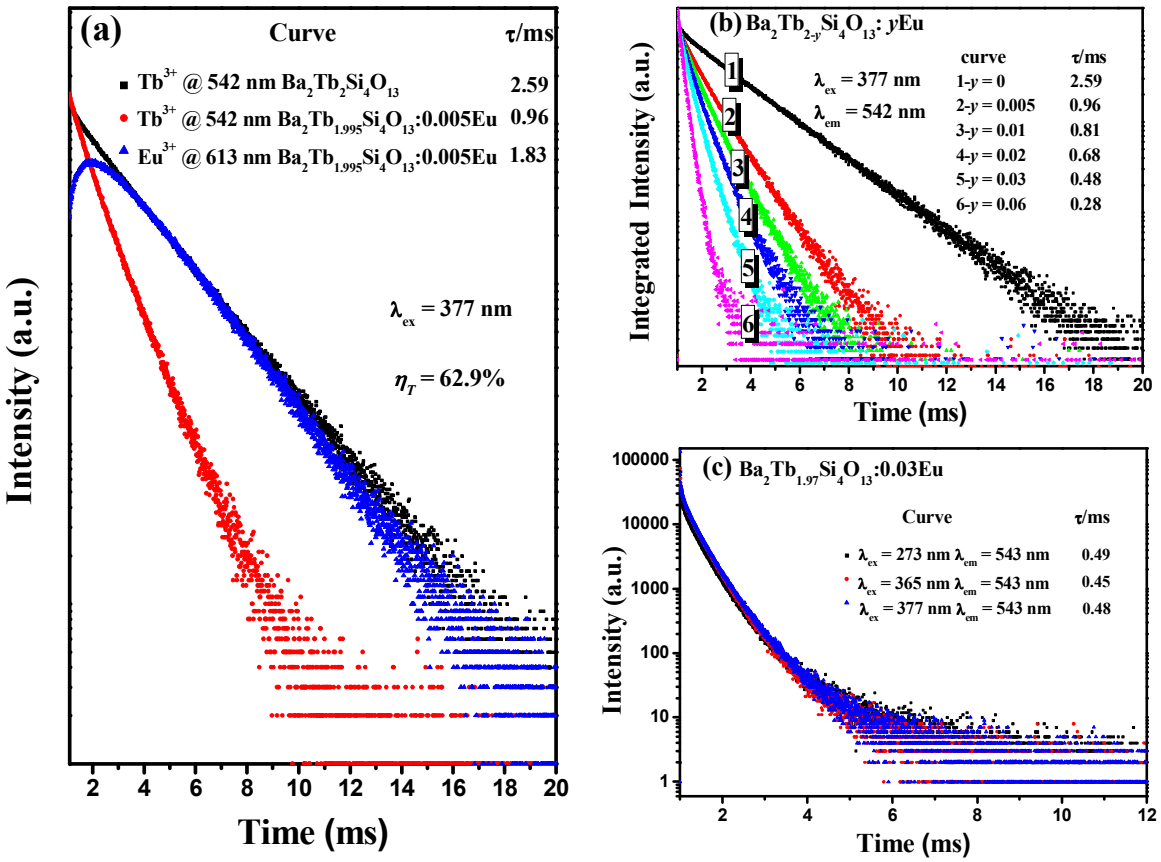

Fig. 8 (a) Decay time curves and lifetimes of Eu^{3+} in $Ba_2Tb_{1.995}Si_4O_{13}$:0.005Eu phosphor and Tb^{3+} in $Ba_2Tb_2Si_4O_{13}$ and $Ba_2Tb_{1.995}Si_4O_{13}$:0.005Eu phosphor. (b) Tb^{3+} decay curves of $Ba_2Tb_{2-y}Si_4O_{13}$:yEu phosphors monitoring 542 nm emission. (c) Tb^{3+} decay curves of $Ba_2Tb_{1.97}Si_4O_{13}$:0.03Eu phosphors monitoring 542 nm emission under 273, 365 and 377 nm excitation.

RSC Advances Accepted Manuscript

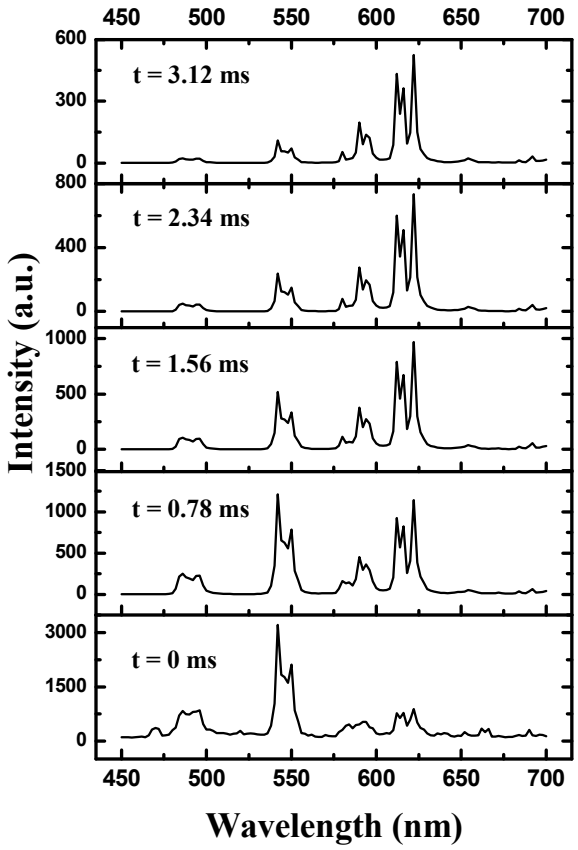

Fig. 9 The time-resolved spectra of $Ba_2Tb_{1.995}Si_4O_{13}$:0.005Eu phosphor under 377 nm excitation.

RSC Advances Accepted Manuscript

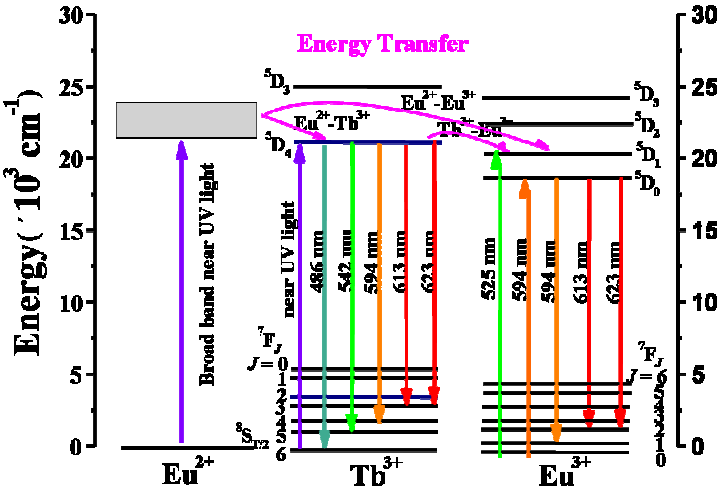

Fig. 10 Energy level model for the ET processes among Eu^{2+}, Tb^{3+}, and Eu^{3+} in $Ba_2Tb_2Si_4O_{13}$ phosphor.

RSC Advances Accepted Manuscript

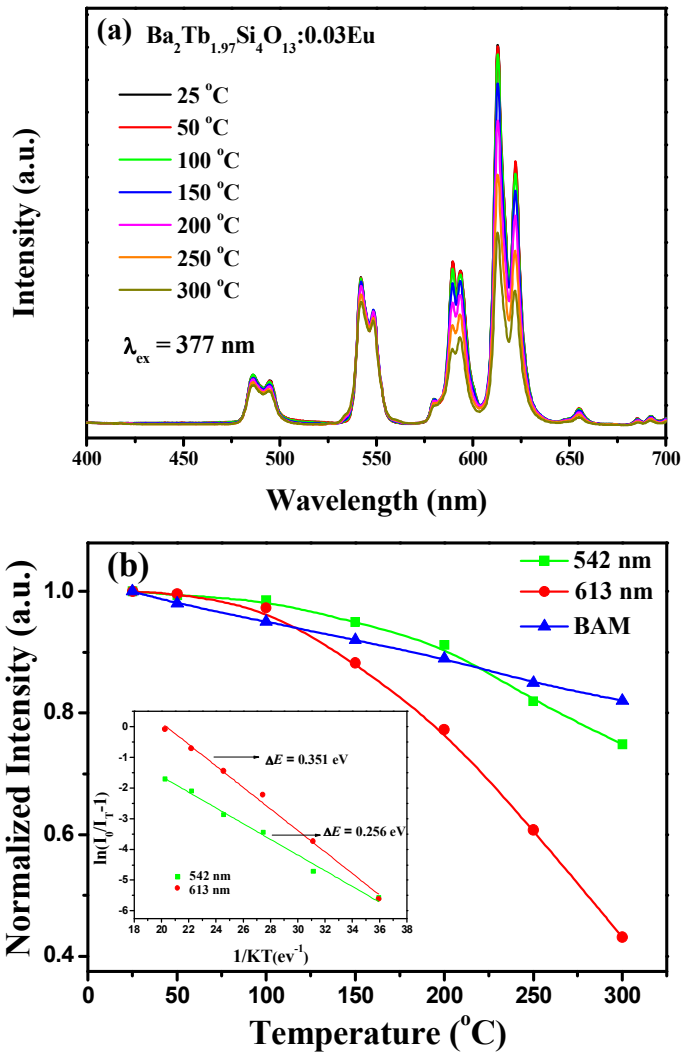

Fig. 11 (a) Temperature-dependent PL spectra of $Ba_2Tb_{1.97}Si_4O_{13}$:0.03Eu. (b) The variations of the relative emission intensities as a function of temperature of the $Ba_2Tb_{1.97}Si_4O_{13}$:0.03Eu phosphor and commercial BAM phosphor. The inset shows relative PL intensities of Tb^{3+}, and Eu^{3+} in $Ba_2Tb_2Si_4O_{13}$ host with raised temperatures. The inset shows the activation energy (ΔE) of Tb^{3+} and Eu^{3+} in $Ba_2Tb_{1.97}Si_4O_{13}$:0.03Eu phosphor.

RSC Advances Accepted Manuscript

Photoluminescence Tuning via Energy Transfer in the Eu-doped $Ba_2(Gd,Tb)_2Si_4O_{13}$ Solid-Solution Phosphors

Jun Zhou[a,b], Zhiguo Xia[*a], Marco Bettinelli[c], Quanlin Liu[a]

Successive energy transfer process Eu^{2+}-Eu^{3+}(Tb^{3+}) and Tb^{3+}-Eu^{3+} appear to occur in the $Ba_2Tb_{2-y}Si_4O_{13}$:yEu (y = 0-0.12) solid-solution phosphors.

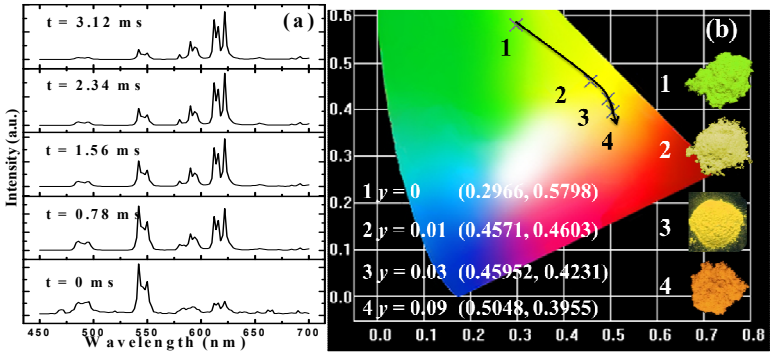

RSC Advances Accepted Manuscript